Research Article

Improving Performance of Spike Pattern Detection Using Close-to-Biology Spiking Neuronal Network

Takuya Nanami, Takashi Kohno
Institute of Industrial Science, The University of Tokyo, Tokyo, Japan

ABSTRACT

In the nervous system, there is a broad variety of neuron types, each exhibiting distinct firing properties. Although these neurons are considered important, the understanding of their role in information processing remains limited. In this study, we constructed a simple network using a piecewise quadratic neuron (PQN) model that can reproduce a variety of neuronal activities. Further, we examined the effect of various neuronal dynamics on the success rate of a biologically plausible spike-pattern detection task. The simulation results showed that certain mathematical structures increased the success rate of spike-pattern detection.

1. Introduction

It has been reported that the nervous system contains a wide variety of neurons, each with diverse neuronal activities. For instance, in response to constant input, neurons in the regular spiking (RS) class show a decline in their firing frequency over time; this process is known as spike-frequency adaptation. In contrast, fast spiking (FS) neurons continue to fire at nearly the same frequency. Elliptic bursting (EB) and parabolic bursting (PB) classes switch between periods of intense firing and resting when exposed to a constant stimulus. Furthermore, Class II neurons in Hodgkin's classification [1] start firing at a relatively high frequency when exposed to a gradually increasing stimulus, whereas Class I neurons start firing at almost zero frequency. Researchers have developed spiking neuron models that reproduce these diverse electrophysiological properties. For example, [2] presented the ionic-conductance-based neuron model that reproduces typical neuron classes in the cortex and thalamus, such as RS, FS, intrinsically bursting (IB), and low-threshold spike (LTS). [3] and [4] reproduced bursting neuron classes, such as elliptic bursting (EB) and parabolic bursting (PB). Additionally, qualitative neuron models that reproduce a variety of neuron classes have also been studied [5], [6], [7]. However, we still do not understand the role of these properties in how the nervous system processes information. This is largely because of the complexity of brain circuits and our limited understanding of how they process information. Moreover, technical hurdles in monitoring the activities of neurons *in vivo* make it challenging to study the contribution of electrophysiological properties in brain function.

In this study, we conducted *in silico* simulations to examine the effect of diverse electrophysiological propertie on the learning task. We employed a simple and biologically plausible network structure proposed in previous studies [8], [9]. The piecewise quadratic neuron (PQN) model [7] was used as the spiking neuron model. This model stands out for its relatively low computational

Corresponding author's E-mail: nanami@iis.u-tokyo.ac.jp, kohno@g.ecc.u-tokyo.ac.jp

demand and capacity to simulate a variety of electrophysiological properties. Its parameters were automatically determined using a fitting method [10], [11] based on metaheuristic algorithms. Despite the multitude of dynamics inherent to neuronal activities, this study primarily focused on the dynamics of the fast subsystem responsible for spike generation. We investigated the effect of changes in the dynamics of the fast subsystem on learning performance.

The organization of the remainder of this paper is as follows: Section 2 presents the methodologies employed, Section 3 discusses the results of our simulations, and Section 4 provides a summary of this work and outlines potential directions for future research.

2. Methods

2.1. *Network model*

Figure 1 illustrates the structure of the constructed network. In this network, the input nodes project to the output neurons through excitatory synapses. In addition, the output neurons inhibit each other through inhibitory synapses. The weights of the excitatory synapses vary depending on the spiking of input nodes and output neurons based on the spike-timing-dependent plasticity (STDP) rule, whereas the weights of the inhibitory synapses are constant. These network structures largely mirror those proposed in the preceding work [9]. The major distinctions are in the model of the output neurons. In contrast with the leaky integrate-and-fire (LIF) model used in [9], we employed the PQN model. In addition, we used a double exponential synapse model, and the number of the input nodes was decreased from 2000 to 512. The stimulus input for the j-th output neuron is given by:

$$I_{j_k} = p_0 \sum_{i=1}^{512} w_{ji}^e x_i - p_1 \sum_{i=1(i \neq j)}^{9} w_{ji}^i s_i \qquad (1)$$

where x_i denotes the activation of the i-th input node with values of 1 or 0. s_i represents the inhibitory synaptic current from the i-th neuron. w_{ji}^e represents the weight of the excitatory synapse from the i-th node to the j-th neuron, whereas w_{ji}^i indicates the weight of the inhibitory synapse from the i-th neuron to the j-th neuron. The parameters p_0 and p_1 determine the impact of the excitatory and inhibitory inputs, respectively.

Figure 2 illustrates an example of the input data, where three distinct spike patterns (represented by blue, green,
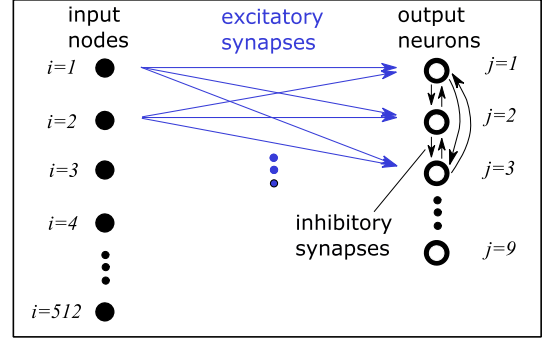
Figure 1. Network structure.
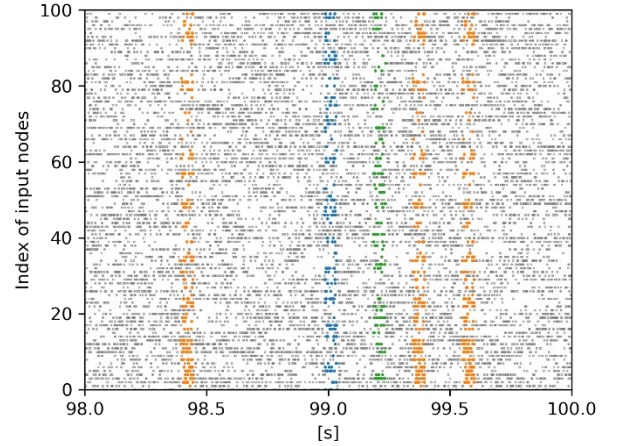
Figure 2. Example of the input data.

and orange dots) are embedded within random spikes (depicted by gray dots). The method of generating the input data was the same as in that used in [9]. Initially, we fed 80 seconds of input data to the network for the learning phase. During this phase, the weights of the excitatory synapses were updated based on the STDP. This was followed by a test phase of 20 seconds to evaluate whether the output neurons detected the embedded spike patterns. A task was deemed successful if all spike patterns were detected by at least one output neuron with a probability of more than 90% during the test phase.

The STDP learning rule at the excitatory synapses is given by

$$\Delta w_{ji}^e = \begin{cases} a^+ \exp\left(\dfrac{t_i - t_j}{\tau^+}\right) & \text{if } t_i \leq t_j, \\ a^- \exp\left(-\dfrac{t_i - t_j}{\tau^-}\right) & \text{if } t_i > t_j. \end{cases} \qquad (2)$$

where t_j and t_j represent the times of the presynaptic and postsynaptic spikes, respectively.

. The parameters τ^- and τ^+ determine the time constant of the long-term depression and potentiation, respectively. The parameters a^+ and a^- control the learning rate.

2.2. Neuron model

The PQN model was designed to support a wide range of neuronal activities with relatively low computational expense. The equations for the PQN model in its two-variable form are given by

$$\frac{dv}{dt} = \frac{\varphi}{\tau}(f(v) - n + I_0 + kI_{stim}), \qquad (3)$$

$$\frac{dn}{dt} = \frac{1}{\tau}(g(v) - n), \qquad (4)$$

$$f(v) = \begin{cases} a_{fn}(v - b_{fn})^2 + c_{fn} & (v < 0) \\ a_{fp}(v - b_{fp})^2 + c_{fp} & (v \geq 0), \end{cases} \qquad (5)$$

$$g(v) = \begin{cases} a_{gn}(v - b_{gn})^2 + c_{gn} & (v < r_g) \\ a_{gp}(v - b_{gp})^2 + c_{gp} & (v \geq r_g), \end{cases} \qquad (6)$$

where v and n denote the membrane potential and recovery variables, respectively. Parameter I_0 is the bias constant. I_{stim} represents the stimulus input, and k is its scaling parameter. The parameters τ and φ are responsible for the time constants of the variables. The parameters r_g, a_x, b_x, and c_x, where x is fn, fp, gn, or gp, control the nullclines of the variables. Constants b_{fp}, c_{fp}, b_{gp}, and c_{gp}, are determined by other parameters to ensure that the nullclines are continuous and smooth (see [7]). The synaptic current was calculated as follows:

$$\frac{ds}{dt} = \begin{cases} \alpha(1 - s) & (v \geq 0) \\ -\beta s & (v < 0), \end{cases} \qquad (6)$$

where s denotes the synaptic current and the parameters α and β determine the time constants. Note that all variables and parameters are entirely abstract and devoid of physical units.

In this study, we focused on two key parameters a_{gn} and φ, which determine the mathematical structure of the fast subsystem. The parameter a_{gn} governs the slope of the left portion of the n-nullcline. For instance, reducing a_{gn} from 0.75 to 0 decreased the slope on the n-nullcline's left portion and shifts the position of the bifurcation point rightwards (Figure 3 (A-B)). The parameter φ adjusts the time constant of v and influences the shape of the stable limit cycle. When φ is increased from

.
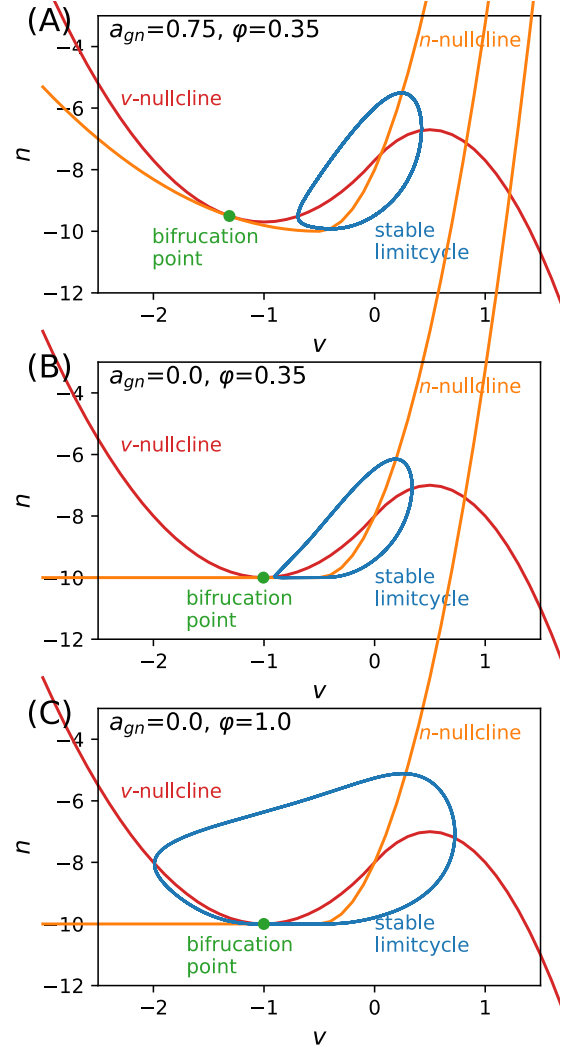
Figure 3. Examples of mathematical structures.
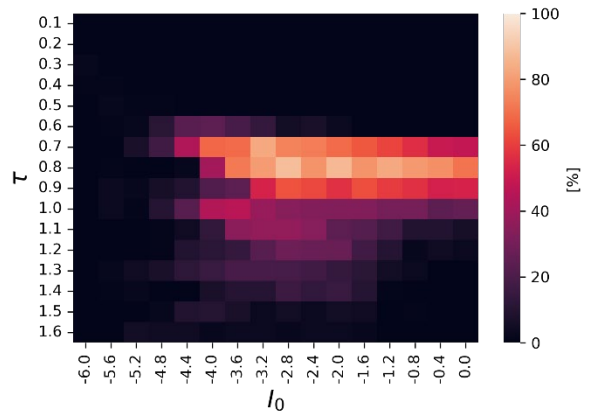
Figure 4. Selection of I_0 and τ for the parameter set $(a_{gn}, \varphi = 0, 1)$.
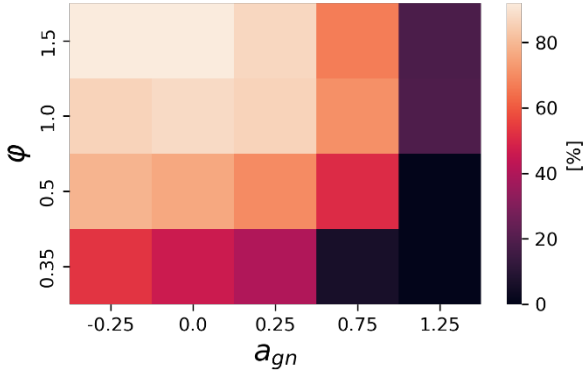
Figure 5. Success rate.
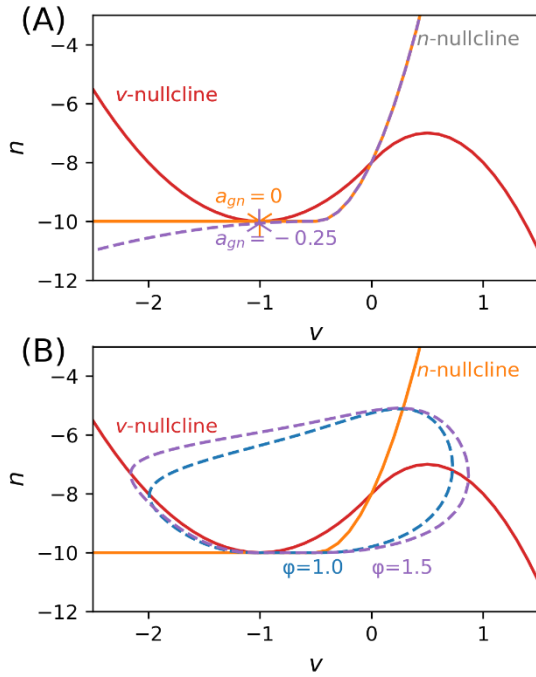
Figure 6. Mathematical structures. (A) Y and inverse Y represent the bifurcation point when a_{gn} is 0 and -0.25, respectively. (B) The blue and purple dotted lines indicate the stable limit cycle when a_{gn} is 1 and 1.5, respectively.

0.35 to 1, the trajectory expands particularly in the negative direction of the v-axis (Figure 3 (B-C)). Our examination encompassed twenty diverse parameter sets, each a unique pairing from a set of five distinct values for a_{gn} (1.75, 0.75, 0.25, 0, and -0.25) and four φ (0.35, 0.5, 1, and 1.5).

In addition, the values of the parameters I_0 and τ were chosen to have the highest success rate in each parameter set. As shown in Figure 4, we calculated the success rate while changing the parameters I_0 and τ with fixed a_{gn}

and φ. The value of I_0 was varied from -6.0 to 0 in increments of 0.4, and the value of τ was varied from 0.1 to 1.6 in increments of 0.1. In total, 256 combinations were examined. For each case, the success rate was calculated by varying the number of patterns from 1 to 5. Twenty trials were conducted for each pattern, resulting in 100 trials. In this case, the success rate was highest at 88% when I_0 and τ were -2.8 and 0.8, respectively, and this value was recorded as the success rate for the parameter set (a_{gn}, $\varphi = 0, 1$).

All other parameters were shared across all parameter sets.

3. Results

The success rates associated with each parameter set are showed in Figure 5. The data suggested a trend: smaller values of a_{gn} and larger values of φ generally yield higher success rates.

4. Conclusion and Discussion

In this work, we devised twenty unique neuronal dynamical structures and examined their influence on the performance of a spatiotemporal pattern detection task. The findings indicated that superior performance was achieved when a_{gn} is smaller and φ is larger. As a_{gn} decreases, the bifurcation point moves closer to $v = 0$. It's important to note that in the PQN network, the point at which v surpasses 0 is regarded as the spike timing for the STDP calculation. This is because the neurotransmitter release initiates when v transcends 0 in our synapse model. If the bifurcation point is in proximity to this point, the neurons tend to fire more quickly. Given the STDP curve's exponential decay nature, these faster-firing neurons are likely to achieve a larger change in synaptic weight compared to their slower-firing counterparts. This could be the reason behind the higher success rates. When a_{gn} was decreased from 0 to -0.25, there was only a slight improvement in the success rate. This was likely because the location of the bifurcation point changed slightly in both cases (Figure 6(A)).

As the parameter φ grows, the trajectory of the stable limit cycle extends further in the negative v-axis direction, thereby increasing the time required for the trajectory to complete a cycle and start a second spike. Given that substantial inputs typically occur instantaneously, these neurons are less likely to produce a second spike. Because a second spike could potentially pair with spike signals unrelated to the target pattern, neurons exhibiting

69

a larger φ are likely to avoid this scenario, thereby achieving the highly reliable target pattern detection. When φ increased from 1 to 1.25, the improvement in success rate was small compared to that when it increased from 0.35 to 0.5 and from 0.5 to 1. This is likely because the shape of the trajectory is generally the same when φ is 1 and when φ is 1.5, and therefore, there is no significant increase in the time taken to reach the second spike (Figure 6(B)).

The results suggest that the following two factors facilitated the success rate. First, the ability to fire quickly in response to a pattern; and second, a longer inter-spike interval during repetitive firing in response to a prolonged stimulus. We plan to test this hypothesis in future studies. For example, we will investigate whether artificially controlling the timing of spiking, apart from the structure of the fast subsystem, improves the success rate. In addition, we will explore the effects of slower dynamics, including bursting and spike-frequency adaptation, on the success rate. Furthermore, we plan to investigate the effect on success rate when each output neuron exhibits different dynamics.

References

1. A. L. Hodgkin, "The local electric changes associated with repetitive action in a non-medulated axon." The Journal of physiology, vol. 107, no. 2, pp. 165–181, Mar. 1948.
2. M. Pospischil, M. Toledo-Rodriguez, C. Monier, Z. Piwkowska, T. Bal, Y. Fregnac, H. Markram, and A. Destexhe, "Minimal hodgkin-huxley type models for different classes of cortical and thalamic neurons", Biological Cybernetics, vol. 99, no. 4-5, pp. 427–441, 2008.
3. X.-J. Wang, "Ionic basis for intrinsic 40 hz neuronal oscillations", NeuroReport, vol. 5, pp. 221–224, 1993.
4. R. E. Plant, "Bifurcation and resonance in a model for bursting nerve cells", Journal of Mathematical Biology, vol. 67, pp. 15–32, 1981.
5. T. Nanami and T. Kohno, "Simple cortical and thalamic neuron models for digital arithmetic circuit implementation", Frontiers in Neuroscience, section Neuromorphic Engineering, vol. 10, no. 181, 2016.
6. T. Nanami, K. Aihara, and T. Kohno, "Elliptic and parabolic bursting in a digital silicon neuron model", in 2016 International Symposium on Nonlinear Theory and Its Applications, November 2016, pp. 198–201.
7. T. Nanami and T. Kohno, "Piecewise Quadratic Neuron model: a tool for close-to-biology spiking neuronal network simulation on dedicated hardware", Frontiers in Neuroscience, section Neuromorphic Engineering, in press.
8. T. Masquelier, R. Guyonneau, and S. J. Thorpe, "Spike timing dependent plasticity finds the start of repeating patterns in continuous spike trains", PLOS ONE, vol. 3, pp. 1–9, 01 2008.
9. T. Masquelier, R. Guyonneau, and S. J. Thorpe, "Competitive STDP-Based Spike Pattern Learning", Neural Computation, vol. 21, no. 5, pp. 1259–1276, 05 2009.
10. T. Nanami, F. Grassia, and T. Kohno, "A parameter optimization method for digital spiking silicon neuron model", Journal of Robotics Networking and Artificial Life, vol. 4, no. 1, pp. 97–101, 2017.
11. T. Nanami, F. Grassia, and T. Kohno, "A metaheuristic approach for parameter fitting in digital spiking silicon neuron model", Journal of Robotics Networking and Artificial Life, vol. 5, no. 1, pp. 32–36, 2018.

Authors Introduction

Dr. Takuya Nanami

He received the Ph.D from University of Tokyo in 2019. He is a research associate in Institute of Industrial Science, University of Tokyo since 2020.

Prof. Takashi Kohno

He received the B.E. degree in medicine (1996) and the Ph.D. degree in mathematical engineering (2002) from University of Tokyo, Japan. He is a professor in Institute of Industrial Science, University of Tokyo since 2018.